Solar Physics
DOI: 10.1007/•••••-•••-•••-••••-•

Oscillation Maps in the Broadband Radio Spectrum of the 1 August 2010 Event

M. Karlický[1] · **J. Rybák**[2]

© Springer ••••

arXiv:1611.02074v1 [astro-ph.SR] 7 Nov 2016

Abstract We search for indications of waves in the 25 – 2000 MHz radio spectrum of the 1 August 2010 event (SOL2010-08-01T08:57:00L075C013), where fast propagating waves in the solar corona with the periods of 181, 69, and 40 seconds were detected in UV observations. Using the wavelet technique we construct a new type of map of oscillations for selected periods in the whole domain of the radio spectrum. While the oscillation with the period of 181 seconds was recognized in the whole 25 – 2000 MHz radio spectrum, oscillations with periods of 69 and 40 seconds were confirmed only in the 250 – 870 MHz frequency range. In the 800 – 2000 MHz range we found periods of 50 and 80 seconds. Moreover, in the 250 – 870 MHz frequency range, the oscillation with the period of about 420 seconds was detected. We also made maps of phases of the 181-second oscillations in order to analyze their frequency drift. At the beginning of the radio event, in the 2000 – 500 MHz frequency range the phase of the 181-second oscillation drifts towards lower frequencies. On the other hand, at frequencies 25 – 500 MHz we found that the phase is nearly synchronous. While the phase drift at higher frequencies can be interpreted as being caused by the UV wave, the synchronization of the phase on lower frequencies is explained by the fast-electron beams, whose acceleration is modulated by the UV wave. Owing to this modulation, the electron beams are accelerated with the period of the UV wave (181 seconds). These beams propagate upwards through the solar corona and generate the 25 – 500 MHz radio emission with the 181-second period. Due to high beam velocity (≈c/3, where c is the light speed) the 25 – 500 MHz radio emission, corresponding to a large interval of heights in the solar corona, is nearly synchronous.

Keywords: Sun: flares — Sun: radio radiation — Sun: oscillations

[1] Astronomical Institute, Academy of Sciences of the Czech Republic, 251 65 Ondřejov, Czech Republic
(e-mail: karlicky@asu.cas.cz)
[2] Astronomical Institute, Slovak Academy of Sciences, SK-05960 Tatranská Lomnica, Slovak Republic
(e-mail: rybak@astro.sk)

1. Introduction

In solar flares, oscillations and waves are commonly observed in radio, X-ray, ultraviolet, and even in γ-ray emissions (Roberts, Edwin, and Benz, 1984; Fárník, Karlický, and Švestka, 2003; Wang *et al.*, 2005; Nakariakov *et al.*, 2006, 2010).

The period of these oscillations ranges from sub-seconds to tens of minutes (Mészárosová *et al.*, 2006; Tan, 2008; Karlický, Zlobec, and Mészárosová, 2010; Kupriyanova *et al.*, 2010; Mészárosová, Rybák, and Karlický, 2011; Huang *et al.*, 2014; Nisticò, Pascoe, and Nakariakov, 2014). Several theoretical models explaining them have been proposed (Nakariakov and Melnikov, 2009).

Various types of oscillations and modes of waves, especially in coronal loops, were already studied numerically (Ofman and Wang, 2002; De Moortel and Hood, 2003; Nakariakov *et al.*, 2004; Nakariakov, Pascoe, and Arber, 2005; Selwa, Murawski, and Solanki, 2005; Jelínek and Karlický, 2009, 2010; Konkol *et al.*, 2010; Ofman, Wang, and Davila, 2012; Pascoe and De Moortel, 2014; Mészárosová *et al.*, 2014).

Very interesting examples of the waves have been presented by Liu *et al.* (2011). Based on the UV images observed by the *Atmospheric Imaging Assembly* (AIA) onboard *Solar Dynamic Observatory* (SDO: Lemen *et al.*, 2012) during the 1 August 2010 flare, the authors showed that these waves are fast-mode magnetosonic waves (having the periods of 181, 69, 40 seconds) propagating with the speed of about 2200 km s^{-1} upwards through the solar corona.

In the present article, for the same event on 1 August 2010, we search for any indication of these waves in the radio spectrum. For this purpose, using the wavelet technique, we constructed a new type of map of oscillations made from the radio spectrum. The maps present power and phase of recognized oscillations. Under the assumption that bursts in the radio spectra are generated by the plasma-emission mechanism (in the frequency range considered here this assumption is commonly accepted), such maps give us information about the distribution of oscillations and waves in the vertical direction in the gravitationally stratified solar atmosphere. A possible frequency drift of the oscillations should express the vertical motion of these oscillations. An attempt to make a similar map, but for sub-second (0.1 second) pulsations during the 11 April 2001 flare, was already made by Karlický, Zlobec, and Mészárosová (2010), but now we use a much more sophisticated and more general method.

The paper is structured as follows: In Sections 2 and 3 we present the data and method. The results are summarized in Section 4, and their analysis and interpretations are in Section 5. Conclusions are given in Section 6.

2. Data

The radio spectrum studied was observed during the 1 August 2010 flare (*Hinode* Flare Catalog - event number 022480 (Watanabe, Masuda, and Segawa, 2012)). This flare, classified as a GOES C3.2 flare, started at 07:25 UT, peaked

at 08:57 UT, and ended at 10:25 UT in NOAA active region 11092 (Liu *et al.*, 2011, 2010; Schrijver and Title, 2011).

The radio spectrum consists of spectra from three radiospectrographs in the time interval of 07:45 – 09:00 UT:

- The *Ondřejov radiospectrograph* located at Ondřejov, Czech Republic. Radiospectrograph frequency range, frequency resolution, and time resolution are 800 – 2000 MHz, 4.7 MHz, and 10 ms, respectively (Jiřička and Karlický, 2008).
- The *Phoenix-4 Bleien radiospectrograph* located at Bleien, Switzerland. Its frequency range, mean frequency resolution, and time resolution are 175 – 870 MHz, 3.61 MHz, and 10 ms, respectively.
- The *IZMIRAN radiospectrograph* located at Troitsk near Moscow, Russia. Its frequency range and time resolution are 25 – 270 MHz and 40 ms, respectively. The frequency range consists of four frequency sub-ranges with different frequency resolutions: 270 – 180 MHz, 1.0 MHz; 180 – 90 MHz, 0.5 MHz; 90 – 45 MHz, 0.25 MHz; and 45 - 25 MHz, 0.14 MHz.

For the analysis performed in this study, all of the data were re-sampled to a temporal sampling convenient for calculations but still small enough to analyze the desired periods of the radio signal: Ondřejov and IZMIRAN radiospectrographs to 2.0 seconds, and Phoenix-4 Bleien radiospectrograph to 2.5 seconds. temporal sampling.

The broadband radio spectrum composed from the radio spectra of all the three radiospectrographs is shown in Figure 1. Black bands show frequencies, where the signal was heavily contaminated by artificial radio noise. These frequencies were excluded from calculations. White areas indicate saturated signals. The radio emission of this flare started at about 7:55 UT in the 250 – 870 MHz range. Then during about 15 minutes the frequency range of this emission increased up to about 2000 – 45 MHz interval. In the 250 – 2000 MHz range it consisted of many fast drifting pulses superimposed on the continuum. The maximum of this burst (BM) slowly drifted from the frequency $\approx$ 500 MHz at 8:22 UT to $\approx$ 350 MHz at 8:50 UT. In the 25 – 270 MHz range the radio pulses were associated with pulsations and Type III bursts superimposed on broadband continuum.

3. Method

Our novel method is based on the wavelet transform (WT), which is suitable for analyzing timeseries containing non-stationary signal at different periods. This property of the WT is due to its functions (wavelets), which are localized both in time and frequency (Daubechies, 1990; Kumar and Foufoula-Georgiou, 1997; Torrence and Compo, 1998). The WT method provides amplitude and phase as well as power of the detected wave-pattern signals. This approach has already been used for analysis of the solar radio signals in several articles by

different groups of authors (*e.g.* Sych and Yan, 2002; Zaqarashvili *et al.*, 2013; Mészárosová, Rybák, and Karlický, 2011; Mészárosová, Karlický, and Rybák, 2011; Mészárosová *et al.*, 2009) and others.

The novelty of our approach is in the way that the essence of the WT results on non-stationary wave-pattern signals is picked up and related to the time–frequency plots of the radio spectra. The resulting parameters or each derived WT, *i.e.* amplitude, phase, and power, can be presented separately within the time–frequency plots of the radio spectra.

Due to possible multiplicity of the non-stationary periodicities that can present simultaneously in the radio signals studied, one has to limit the investigated periodicities either to that of maximum power in the general WT period range or to a narrower WT period range of particular interest. Both calculated significance of the derived WT periodicities and cone-of-influence can be taken into account in our novel approach.

The method can be applied to any 2D time–frequency radio spectrogram. The method is described in few consecutive steps given below:

i) A linear trend of the radio signal, derived from the first and last values of the time series, is subtracted separately from discrete data of all radio signal time series in the 2D time–frequency radio spectrogram. This operation keeps the first and last values of the series close to zero.

ii) The WT of the adapted data of each individual radio-signal time series is performed using the pre-selected mother wavelet type and its parameters (period (scale) range and sampling, significance level resulting in the 2D WT amplitude, phase and power in the time-period domain).

iii) The WT power spectra of all individual radio time series are checked for occurrence of local power maxima in each temporal moment of the time series. The WT results (power, amplitude, phase, significance) are taken together with the radio frequency, time, and the WT period information for all such WT power maxima locations detected. These local maxima have to be distinguished with a clear decrease of the power to lower/higher periods.

iv) A histogram of the selected WT period results of the WT power local maxima above a certain significance level is created from all individual radio time series of the 2D time–frequency radio spectrogram. This histogram is used for specifying a selected period range $[p_1, p_2]$ where a sufficiently large number of period results are grouped in the period range of interest.

v) The WT power local maxima results whose WT periods are localized within the selected period ranges $[p_1, p_2]$ and their WT power is above the specified significance level are identified. Such WT (amplitude, period, power) results are chosen for their time–frequency positions in the 2D time–frequency radio spectrogram.

vi) These WT results can be then over-plotted on the original radio spectrum plots.

The method described allows us to clearly identify frequencies where the wave-pattern in the selected period range $[p_1, p_2]$ really exists, including its temporal location and span. Moreover, this presentation of the identified frequencies/time/period locations opens a possibility to select one of the resulting WT parameters to be plotted on top of the radiospectrogram. We would like to point out that all WT calculations are performed on the individual radio spectrum time series independently. Therefore a smooth behavior of the selected WT resulting parameter over the identified frequency–time domain with significant wave-pattern in the selected period range $[p_1, p_2]$ shows the reliability of the derived WT results once the parameters of the WT are specified reasonably.

Finally we have to mention the actual parameters of the WT used in this study. The Morlet mother wavelet, consisting of a complex sine wave modulated by a Gaussian, was selected to search for radio signal variability at different periods. The non-dimensional frequency ω_0, equal to 6 was taken to satisfy the admissibility condition (Farge, 1992). The WT has been calculated for the period range from 10 to 600 seconds with scales sampled as fractional powers of two with $\delta j = 0.4$ still small enough to give an adequate sampling in scale, a minimum scale $s_j = 9.64\,\mathrm{s}$ and a number of scales $N = 101$. As the basis of all calculations the WT computational algorithm of Torrence and Compo (1998) was applied to individual radio-signal time series.

Due to the WT algorithm applied, the wavelet power spectra are suppressed within a cone of influence (Torrence and Compo, 1998). The cones are indicated in our WT results plots by cross-hatched regions. Nevertheless, because we minimize the radio signal at the beginning/end of the individual radio time series we take into account all significant WT results, even those located within the aforementioned cones of influence.

The significance level of the derived wavelet power spectrum was derived using the null hypothesis according to Torrence and Compo (1998) assuming that the time series has a mean power spectrum. If a wavelet power spectrum is well above the background mean power spectrum, it can be assumed to be real with a certain confidence level. The 95 % confidence level, used in this study, implies that 5 % of the wavelet power should be above this level for each scale. The global wavelet spectrum was used as an estimate of the background mean power spectrum against which the significance of the local wavelet power spectrum features can be tested (Percival, 1995; Kestin *et al.*, 1998).

The abovedescribed method finally allows us to identify and display the significantly strong wave-pattern signals in the whole 2D time–frequency domain of the radio spectrogram. The identified wave-pattern signals are of the power which peaks within the selected period range for the particular temporal moment and investigated radio frequency. Advantages of our novel method are that it provides a clear way to detect time–frequency evolution of the radio signal wave-pattern appearance and at the same time to follow the time–frequency distribution of the period, amplitude, and phase of those wave-patterns. From the WT results over-plots on the original radio spectrograms change of the periods, strength, and phase (frequency drift) of the wave-pattern signals can be derived for interpretation of the radio source properties.

4. Results

Using the abovedescribed method we analyzed the radio spectra presented in Figure 1. First, from radio-flux time series at all frequencies of studied radio spectrum, we computed the wavelet power, wavelet amplitude, and wavelet phase spectra. An example of such computations for the radio flux on the 1600 MHz frequency, taken from the 800 – 2000 MHz Ondřejov radio spectrum, is shown in Figure 2. These wavelet spectra show the period of about 180 seconds and periods above 300 seconds.

Then, using such results for all frequencies in the selected radio spectrum, we computed the histograms of all periods in this radio spectrum corresponding to the well-defined local maxima of the WT power. Results for IZMIRAN, Phoenix-4, and Ondřejov radio spectra are shown in Figure 3. The dotted vertical lines indicate the periods 181, 69, and 40 seconds, which were detected in UV observations (Liu *et al.*, 2011). As seen here, while the oscillation with the period of 181 seconds was recognized in the whole 25 – 2000 MHz radio spectrum, oscillations with the periods of 69 and 40 seconds were confirmed only in the 250 – 870 MHz frequency range. In the 800 – 2000 MHz range we found periods of 50 and 80 seconds. Moreover, in the 250 – 870 MHz frequency range, the oscillation with the period of about 420 seconds was detected.

The most distinct period found both in the UV and radio observations is the period 181 seconds. Therefore, in Figures 4 and 5 we present wavelet results computed for the period interval around this period, namely for the interval 160 –220 seconds (the cross-hatched areas in Figure 3).

Figure 4 shows the radio spectra recorded by the IZMIRAN, Phoenix-4, and Ondřejov radiospectrographs over-plotted by light-blue areas, where the significant WT power for the period interval around 181 seconds was found. On the other hand, Figure 5 shows the radio spectra over-plotted by the areas as in Figure 4, but with the pink bands expressing the wave phase. The black borders of these bands indicate zero phase. Note that at areas of saturated data no periods and wave phases can be detected.

As seen in Figure 5 the phase of the 181 second oscillation in this global map appears to be nearly synchronized over the whole 25 – 2000 MHz frequency range. However, a detailed view of some parts of the radio spectrum show a more complex situation with drifts of the oscillation phase. For example, at the beginning of the radio event in the time interval of 08:12 – 08:18 UT, the zero oscillation phase drifts from the frequency 2000 MHz at 08:13:52 UT, to 500 MHz at 08:15:15 UT (Figure 6). The mean frequency drift of this phase is about -18 MHz s^{-1}. At lower frequencies, the phase of the oscillations is more or less synchronized. For comparison see Figure 7, showing the original radio spectrum in the same time and frequency intervals,.

Besides the most distinct period of 181 seconds, found both in the UV and radio observations, we have analyzed also the time–frequency localization of the less dominant period of ≈69 seconds. Here we can state that this period is highly synchronized as in the case of the most dominant period in the period range 500 – 870 MHz. The temporal span of the period occurrence is a little different.

Table 1. Frequencies [f] and time difference [Δt] for the drifting zero wave phase starting at 08:13:52 UT taken from Figure 6, and corresponding electron densities n_e (F-fundamental, H-harmonic) and propagation distance [D_w] of the UV wave with the velocity of $v_w = 2200$ km s^{-1}.

$(f_1 - f_2)$ [MHz]	$\Delta t(f_1 - f_2)$ [s]	$n_e(f_1)$ [cm^{-3}]	$n_e(f_2)$ [cm^{-3}]	$D_w = v_w \Delta t$ [km]
2000 – 500	83	4.93×10^{10} (F)	3.08×10^{9} (F)	182,600
2000 – 500	83	1.23×10^{10} (H)	7.72×10^{8} (H)	182,600

Table 2. Heights [h] and distances [D_{Asch}] according to the Aschwanden model of the solar atmosphere for the plasma emission of the radio sources at 2000 and 500 MHz and time delays of propagation of the UV wave [Δt_w] ($v_w = 2200$ km s^{-1}) along these distances.

f [MHz]	h [km]	D_{Asch} [km]	Δt_w [s]
Fundamental			
2000	8,250		
500	26,450	18,200	8.3
Harmonic			
2000 (1000)	14,770		
500 (250)	47,370	32,600	14.8

5. Analysis and Interpretation

Now, let us analyze the phase drift, presented in Figure 6, in more detail. For this analysis we assume that the observed radio burst is generated by the plasma emission mechanism, *i.e.* the electron plasma density can be determined from the observed frequency as equal to the plasma or double plasma frequency (emission on the fundamental (F) or harmonic (H) frequency).

Considering the above mentioned frequencies and times of the zero phase we calculated the electron plasma densities in the radio sources at 2000 and 500 MHz. Then assuming that the phase drift is caused by the wave observed in UV with the velocity $v_w = 2200$ km s^{-1}, we calculated the distance [D_w] of the UV wave propagation. The calculated plasma densities and distances are shown in Table 1.

Now, let us compare these distances with those in density models of the solar atmosphere, *e.g.* models proposed by Allen (1947); Newkirk (1961); Maxwell and Thompson (1962); Palmer (1974); Mann *et al.* (1999); Aschwanden (2002). However, for the radio emission in the 500 – 2000 MHz range only the Aschwanden model can be used. (Other models we will consider in the analysis of the radio emission at frequencies below 500 MHz.)

Table 3. Distances [D] between heights, corresponding to 500 MHz and 25 MHz plasma emission in the Aschwanden (Asch), 10× Baumbach-Allen (10BA), and 4× Newkirk (4N) models of the solar atmosphere. Times [t] mean those for propagation of the electron beam with the velocity c/3.

$D_{\rm Asch}$ [km]	$t_{\rm Asch}$ [s]	$D_{\rm 10BA}$ [km]	$t_{\rm 10BA}$ [s]	$D_{\rm 4N}$ [km]	$t_{\rm 4N}$ [s]
Fundamental					
255,600	2.55	965,400	9.65	1,103,300	11.03
Harmonic					
330,400	3.30	1,298,300	12.98	2,015,200	20.15

Thus, we compare the distances shown in Table 1 with those in the density model by Aschwanden (2002); the heights and distances are shown in Table 2, together with the propagation times of the UV wave ($v_{\rm w} = 2200$ km s^{-1}) along these distances. As seen in Tables 1 and 2, the distance [$D_{\rm w}$] is much greater than distances in the Aschwanden atmospheric model [$D_{\rm Asch}$]; compare also $\Delta t(f_1 - f_2)$ and $\Delta t_{\rm w}$. If we accept the idea that this phase drift is caused by the wave observed in the UV, then there are two possible explanations: i) the real density profile of the solar atmosphere differs essentially from that in the Aschwanden model or ii) the angle between the UV wave propagation and vertical direction in the solar atmosphere is large ($\approx 80°$). Because the locations of radio sources are not known, we need to consider both explanations, but based on the UV wave images it appears that the first explanation is more probable. Note that combination of the two explanations is also possible. Moreover, deviations from the Aschwanden model may be due to density changes at the beginning of the flare.

Furthermore, Figure 6 shows that in the 25 – 500 MHz frequency range the oscillation phase is more or less synchronized. The corresponding distances in the Aschwanden, 10× Baumbach–Allen (10BA), and 4× Newkirk models are shown in Table 3. The UV wave is too slow to explain this synchronization at such large distances. Thus, it appears that only the possible explanation of this synchronization is the electron beams, whose acceleration is modulated by the UV wave, somewhere in the deep and dense layers of the solar atmosphere. Owing to this modulation, the electron beams are accelerated with the period of the UV wave (181 seconds). These beams propagate upwards through the solar corona and generate the 25 – 500 MHz radio emission with the 181 seconds period. Due to high beam velocity, the 25 – 500 MHz radio emission, corresponding to a large interval of heights in the solar corona, is nearly synchronized. If we assume the beam velocity as $\approx$c/3 = 100,000 km s^{-1}, where c is the light speed, then the Aschwanden model is the best of the models considered for explanation of the 25 – 500 MHz synchronization within a few seconds; see the times in Table 3. This explanation can be supported by Type III bursts observed in the 25 – 270 MHz range in the radio spectrum, as shown in Figure 7.

As concerns other parts of the phase map (Figure 5), some drifts at higher frequencies can be explained by the propagation of the UV wave and synchronization of the oscillation phase at lower frequencies (higher altitudes in the solar atmosphere) by Type III electron beams.

Finally, we estimated the velocity of the agent generating the maximum burst drift (BM), observed in the 08:22 – 08:50 UT interval. Using all of above mentioned models, the velocity was estimated as 6 – 46 km s^{-1}. Because this velocity is too slow, it appears that it expresses a growth of the flaring magnetic-field structure during this time interval.

6. Conclusions

In order to search for radio signatures of the UV waves that were observed in the 1 August 2010 event, we constructed a new type of map using the wavelet technique applied on the broadband 25 – 2000 MHz radio spectrum.

An analysis of UV observations during the 1 August 2010 event revealed periods of 181, 69, and 40 seconds. In the present article, in the radio range, we found the same periods: i) The oscillation with the period of 181 seconds was found in the whole 25 – 2000 MHz radio spectrum, and ii) the oscillations with the periods of 69 and 40 seconds were only in the 250 – 870 MHz range. Moreover, in the 800 – 2000 MHz frequency range we found periods of 50 and 80 seconds, and in the 250 – 870 MHz range, an oscillation with a 420-second period.

We made maps of phases of the 181 second oscillations in order to analyze their frequency drift. Namely, assuming that the plasma emission mechanism generated the radio bursts in the 1 August 2010 event, the drift of the oscillation phase can be interpreted as caused by the UV wave propagating upwards (negative frequency drift) or downwards (positive frequency drift) through the solar atmosphere.

We found that at the beginning of the radio event, in the 2000 – 500 MHz frequency range, the phase of the 181-second oscillation drifts towards lower frequencies. This drift we interpreted as caused by the propagating UV wave. However, because the travel distance of the UV wave with the velocity $v_w = 2200$ km s^{-1} is much greater than the height differences (corresponding to the 2000 – 500 MHz frequencies) in the model of the solar atmosphere by Aschwanden (2002), we propose that in this case the real electron=density profiles differs from that in the Aschwanden model or the propagation direction of the UV wave deviates substantially from vertical direction in the solar atmosphere. Based on the UV wave images, it appears that the first explanation is more probable. Note that combination of the both explanations is also possible. Moreover, deviations from the Aschwanden model may be due to density changes at the beginning of the flare.

On the other hand, at frequencies below 500 MHz we found that the phase is more or less synchronized (within a few seconds). We propose that this phase synchronization is caused by electron beams, of which the acceleration is modulated by the UV wave, somewhere in the deep and dense layers of the solar atmosphere.

Owing to this modulation, the electron beams are accelerated with the period of the UV wave (181 seconds). These beams propagate upwards through the solar corona and generate the 25 – 500 MHz radio emission with the 181-second period. Due to high beam velocity, the 25 – 500 MHz radio emission, corresponding to a large range of heights in the solar corona, is nearly synchronized. If we assume the beam velocity as $\approx$c/3, where c is the light speed, then the Aschwanden model is the best of the models considered for an explanation of the 25 – 500 MHz synchronization within a few seconds. Type III bursts observed in this range speak in favour of this interpretation.

Finally, while the processes of modulation of the electron beam acceleration by magnetosonic waves were considered in several articles,*e.g.*, by Nakariakov *et al.* (2016), the process of generation or modulation of the plasma radio emission by the UV wave is unclear. Maybe, at some locations the propagating UV (fast magnetosonic) wave is changed to a weak magnetosonic shock or accompanied by it. The shock accelerates electrons, of which the distribution function is unstable for plasma waves producing radio emission, similarly to that in Type II burst. Another possibility is that the density variations modify the optical thickness of the radio emission, especially for the emission close to the plasma frequency.

Acknowledgments The authors thank an anonymous referee for useful comments. Furthermore, the authors thank V. Fomichev and R. Gorgutsa for providing of the IZMIRAN data. This research was supported by the grants P209/12/0103 (GA ČR) and the project RVO:67985815 of the Astronomical Institute of the Academy of Sciences. This work was supported by the Science Grant Agency project VEGA 2/0004/16 (Slovakia). Help of the Bilateral Mobility Project SAV-16-03 of the SAS and CAS is acknowledged. This article was created by the realization of the project ITMS No.26220120009, based on the supporting operational Research and development program financed from the European Regional Development Fund. This research has made use of NASA's Astrophysics Data System. The wavelet analysis was performed with software based on tools provided by C. Torrence and G. P. Compo at `paos.colorado.edu/research/wavelets`.

Disclosure of Potential Conflicts of Interest

The authors declare that they have no conflicts of interest.

References

Allen, C.W.: 1947, Interpretation of Electron Densities from Corona Brightness. *Mon. Not. Roy. Astron. Soc.* **107**, 426. DOI. ADS.

Aschwanden, M.J.: 2002, Particle acceleration and kinematics in solar flares - A Synthesis of Recent Observations and Theoretical Concepts (Invited Review). *Space Sci. Rev.* **101**, 1. DOI. ADS.

Daubechies, I.: 1990, The wavelet transform, time-frequency localization and signal analysis. *IEEE Transactions on Information Theory* **36**, 961. ADS.

De Moortel, I., Hood, A.W.: 2003, The damping of slow MHD waves in solar coronal magnetic fields. *Astron. Astrophys.* **408**, 755. DOI. ADS.

Farge, M.: 1992, Wavelet transforms and their applications to turbulence. *Ann. Rev. Fluid Mech.* **24**, 395. DOI. ADS.

Fárník, F., Karlický, M., Švestka, Z.: 2003, Hard x-ray Pulsations in the Initial Phase of Flares. *Solar Phys.* **218**, 183. DOI. ADS.

Huang, J., Tan, B., Zhang, Y., Karlický, M., Mészárosová, H.: 2014, Quasi-Periodic Pulsations with Varying Period in Multi-Wavelength Observations of an X-class Flare. *Astrophys. J.* **791**, 44. DOI. ADS.

Jelínek, P., Karlický, M.: 2009, Computational study of impulsively generated standing slow acoustic waves in a solar coronal loop. *European Phys. J. D* **54**, 305. DOI. ADS.

Jelínek, P., Karlický, M.: 2010, Impulsively Generated Wave Trains in a Solar Coronal Loop. *IEEE Transactions on Plasma Science* **38**, 2243. DOI. ADS.

Jiřička, K., Karlický, M.: 2008, Narrowband Pulsating Decimeter Structure Observed by the New Ondřejov Solar Radio Spectrograph. *Solar Phys.* **253**, 95. DOI. ADS.

Karlický, M., Zlobec, P., Mészárosová, H.: 2010, Subsecond (0.1 s) Pulsations in the 11 April 2001 Radio Event. *Solar Phys.* **261**, 281. DOI. ADS.

Kestin, T.S., Karoly, D.J., Yano, J.-I., Rayner, N.A.: 1998, Time-Frequency Variability of ENSO and Stochastic Simulations. *J. Climate* **11**, 2258. DOI. ADS.

Konkol, P., Murawski, K., Lee, D., Weide, K.: 2010, Numerical simulations of the attenuation of the fundamental slow magnetoacoustic standing mode in a gravitationally stratified solar coronal arcade. *Astron. Astrophys.* **521**, A34. DOI. ADS.

Kumar, P., Foufoula-Georgiou, E.: 1997, Wavelet analysis for geophysical applications. *Rev. Geophys.* **35**, 385. DOI. ADS.

Kupriyanova, E.G., Melnikov, V.F., Nakariakov, V.M., Shibasaki, K.: 2010, Types of Microwave Quasi-Periodic Pulsations in Single Flaring Loops. *Solar Phys.* **267**, 329. DOI. ADS.

Lemen, J.R., Title, A.M., Akin, D.J., Boerner, P.F., Chou, C., Drake, J.F., Duncan, D.W., Edwards, C.G., Friedlaender, F.M., Heyman, G.F., Hurlburt, N.E., Katz, N.L., Kushner, G.D., Levay, M., Lindgren, R.W., Mathur, D.P., McFeaters, E.L., Mitchell, S., Rehse, R.A., Schrijver, C.J., Springer, L.A., Stern, R.A., Tarbell, T.D., Wuelser, J.-P., Wolfson, C.J., Yanari, C., Bookbinder, J.A., Cheimets, P.N., Caldwell, D., Deluca, E.E., Gates, R., Golub, L., Park, S., Podgorski, W.A., Bush, R.I., Scherrer, P.H., Gummin, M.A., Smith, P., Auker, G., Jerram, P., Pool, P., Soufli, R., Windt, D.L., Beardsley, S., Clapp, M., Lang, J., Waltham, N.: 2012, The Atmospheric Imaging Assembly (AIA) on the Solar Dynamics Observatory (SDO). *Solar Phys.* **275**, 17. DOI. ADS.

Liu, R., Liu, C., Wang, S., Deng, N., Wang, H.: 2010, Sigmoid-to-flux-rope Transition Leading to a Loop-like Coronal Mass Ejection. *Astrophys. J. Lett.* **725**, L84. DOI. ADS.

Liu, W., Title, A.M., Zhao, J., Ofman, L., Schrijver, C.J., Aschwanden, M.J., De Pontieu, B., Tarbell, T.D.: 2011, Direct Imaging of Quasi-periodic Fast Propagating Waves of ˜2000 km s^{-1} in the Low Solar Corona by the Solar Dynamics Observatory Atmospheric Imaging Assembly. *Astrophys. J. Lett.* **736**, L13. DOI. ADS.

Mann, G., Jansen, F., MacDowall, R.J., Kaiser, M.L., Stone, R.G.: 1999, A heliospheric density model and type III radio bursts. *Astron. Astrophys.* **348**, 614. ADS.

Maxwell, A., Thompson, A.R.: 1962, Spectral Observations of Solar Radio Bursts. II. Slow-Drift Bursts and Coronal Streamers. *Astrophys. J.* **135**, 138. DOI. ADS.

Mészárosová, H., Karlický, M., Rybák, J.: 2011, Magnetoacoustic Wave Trains in the 11 July 2005 Radio Event with Fiber Bursts. *Solar Phys.* **273**, 393. DOI. ADS.

Mészárosová, H., Rybák, J., Karlický, M.: 2011, Separation of drifting pulsating structures in a complex radio spectrum of the 2001 April 11 event. *Astron. Astrophys.* **525**, A88. DOI. ADS.

Mészárosová, H., Karlický, M., Rybák, J., Fárník, F., Jiřička, K.: 2006, Long period variations of dm-radio and X-ray fluxes in three X-class flares. *Astron. Astrophys.* **460**, 865. DOI. ADS.

Mészárosová, H., Karlický, M., Rybák, J., Jiřička, K.: 2009, Tadpoles in Wavelet Spectra of a Solar Decimetric Radio Burst. *Astrophys. J. Lett.* **697**, L108. DOI. ADS.

Mészárosová, H., Karlický, M., Jelínek, P., Rybák, J.: 2014, Magnetoacoustic Waves Propagating along a Dense Slab and Harris Current Sheet and their Wavelet Spectra. *Astrophys. J.* **788**, 44. DOI. ADS.

Nakariakov, V.M., Melnikov, V.F.: 2009, Quasi-Periodic Pulsations in Solar Flares. *Space Sci. Rev.* **149**, 119. DOI. ADS.

Nakariakov, V.M., Pascoe, D.J., Arber, T.D.: 2005, Short Quasi-Periodic MHD Waves in Coronal Structures. *Space Sci. Rev.* **121**, 115. DOI. ADS.

Nakariakov, V.M., Tsiklauri, D., Kelly, A., Arber, T.D., Aschwanden, M.J.: 2004, Acoustic oscillations in solar and stellar flaring loops. *Astron. Astrophys.* **414**, L25. DOI. ADS.

Nakariakov, V.M., Foullon, C., Verwichte, E., Young, N.P.: 2006, Quasi-periodic modulation of solar and stellar flaring emission by magnetohydrodynamic oscillations in a nearby loop. *Astron. Astrophys.* **452**, 343. DOI. ADS.

Nakariakov, V.M., Inglis, A.R., Zimovets, I.V., Foullon, C., Verwichte, E., Sych, R., Myagkova, I.N.: 2010, Oscillatory processes in solar flares. *Plasma Phys. Controlled Fusion* **52**(12), 124009. DOI. ADS.

Nakariakov, V.M., Pilipenko, V., Heilig, B., Jelínek, P., Karlický, M., Klimushkin, D.Y., Kolotkov, D.Y., Lee, D.-H., Nisticò, G., Van Doorsselaere, T., Verth, G., Zimovets, I.V.: 2016, Magnetohydrodynamic Oscillations in the Solar Corona and Earth's Magnetosphere: Towards Consolidated Understanding. *Space Sci. Rev.* **200**, 75. DOI. ADS.

Newkirk, G. Jr.: 1961, The Solar Corona in Active Regions and the Thermal Origin of the Slowly Varying Component of Solar Radio Radiation. *Astrophys. J.* **133**, 983. DOI. ADS.

Nisticò, G., Pascoe, D.J., Nakariakov, V.M.: 2014, Observation of a high-quality quasi-periodic rapidly propagating wave train using SDO/AIA. *Astron. Astrophys.* **569**, A12. DOI. ADS.

Ofman, L., Wang, T.: 2002, Hot Coronal Loop Oscillations Observed by SUMER: Slow Magnetosonic Wave Damping by Thermal Conduction. *Astrophys. J. Lett.* **580**, L85. DOI. ADS.

Ofman, L., Wang, T.J., Davila, J.M.: 2012, Slow Magnetosonic Waves and Fast Flows in Active Region Loops. *Astrophys. J.* **754**, 111. DOI. ADS.

Palmer, I.D.: 1974, A type II solar radio burst observed in the corona and in interplanetary space. *Solar Phys.* **37**, 443. DOI. ADS.

Pascoe, D.J., De Moortel, I.: 2014, Standing Kink Modes in Three-dimensional Coronal Loops. *Astrophys. J.* **784**, 101. DOI. ADS.

Percival, D.P.: 1995, On estimation of the wavelet variance. *Biometrika* **82**, 619.

Roberts, B., Edwin, P.M., Benz, A.O.: 1984, On coronal oscillations. *Astrophys. J.* **279**, 857. DOI. ADS.

Schrijver, C.J., Title, A.M.: 2011, Long-range magnetic couplings between solar flares and coronal mass ejections observed by SDO and STEREO. *J. Geophys. Res. (Space Phys.)* **116**, A04108. DOI. ADS.

Selwa, M., Murawski, K., Solanki, S.K.: 2005, Excitation and damping of slow magnetosonic standing waves in a solar coronal loop. *Astron. Astrophys.* **436**, 701. DOI. ADS.

Sych, R.A., Yan, Y.-H.: 2002, Wavelet Cleaning of Solar Dynamic Radio Spectrograms. *Chin. J. Astron. Astrophys.* **2**, 183. ADS.

Tan, B.: 2008, Observable Parameters of Solar Microwave Pulsating Structure and Their Implications for Solar Flare. *Solar Phys.* **253**, 117. DOI. ADS.

Torrence, C., Compo, G.P.: 1998, A Practical Guide to Wavelet Analysis. *Bull. Am. Meteor. Soc.* **79**, 61. DOI. ADS.

Wang, T.J., Solanki, S.K., Innes, D.E., Curdt, W.: 2005, Initiation of hot coronal loop oscillations: Spectral features. *Astron. Astrophys.* **435**, 753. DOI. ADS.

Watanabe, K., Masuda, S., Segawa, T.: 2012, Hinode Flare Catalogue. *Solar Phys.* **279**, 317. DOI. ADS.

Zaqarashvili, T.V., Melnik, V.N., Brazhenko, A.I., Panchenko, M., Konovalenko, A.A., Franzuzenko, A.V., Dorovskyy, V.V., Rucker, H.O.: 2013, Radio seismology of the outer solar corona. *Astron. Astrophys.* **555**, A55. DOI. ADS.

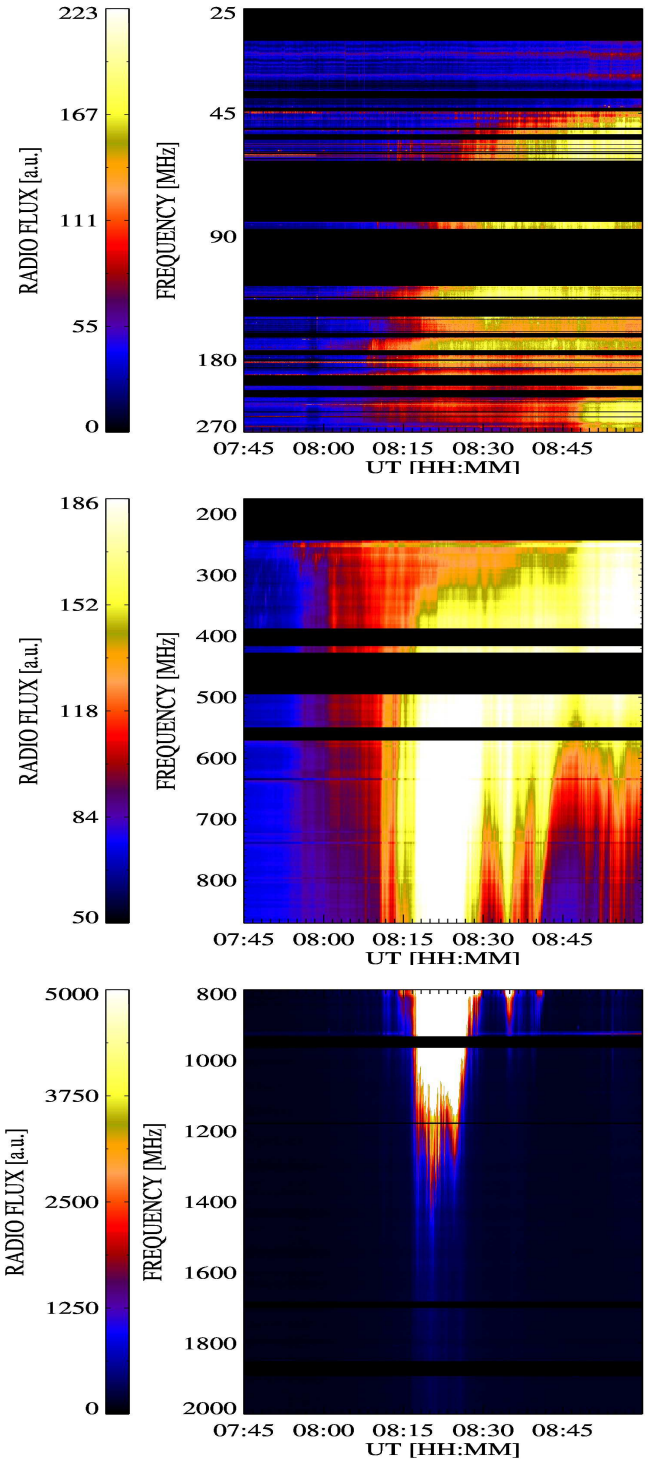

Figure 1. Radio spectra recorded by the IZMIRAN (top), Phoenix-4 (middle), and Ondřejov (bottom) radiospectrographs for the common time interval 07:45 – 09:00 UT on 1 August 2010. Black-horizontal bands mark the data omitted from calculations due to presence of radio noise. White areas in the Phoenix-4 and Ondřejov radio spectra indicate saturated signal data.

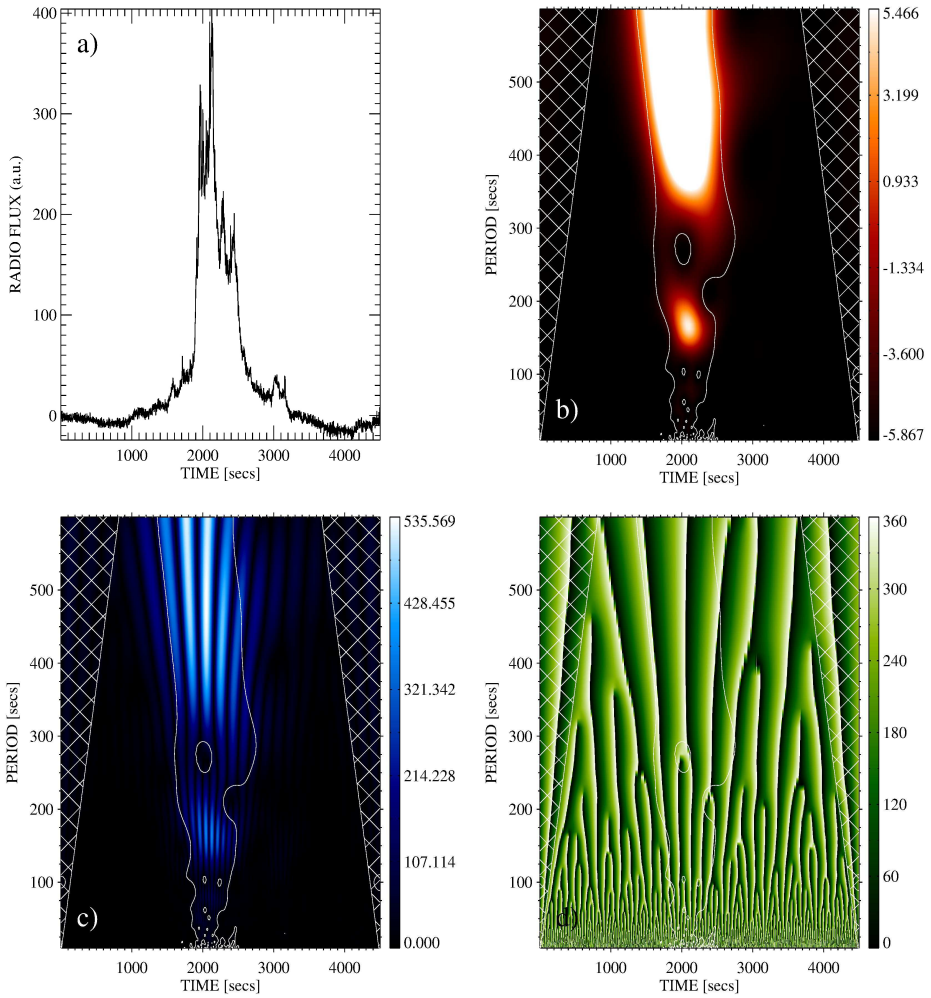

Figure 2. Example of the analysis of the radio-signal time series taken from the Ondřejov radio spectrum at the frequency 1600 MHz: a) radio flux *vs.* time with a background subtracted, b) WT power, c) WT amplitude, and d) WT phase. White contours in b) and c) mark results above the selected significance level and white cross-hatched areas designate areas outside the cone of influence.

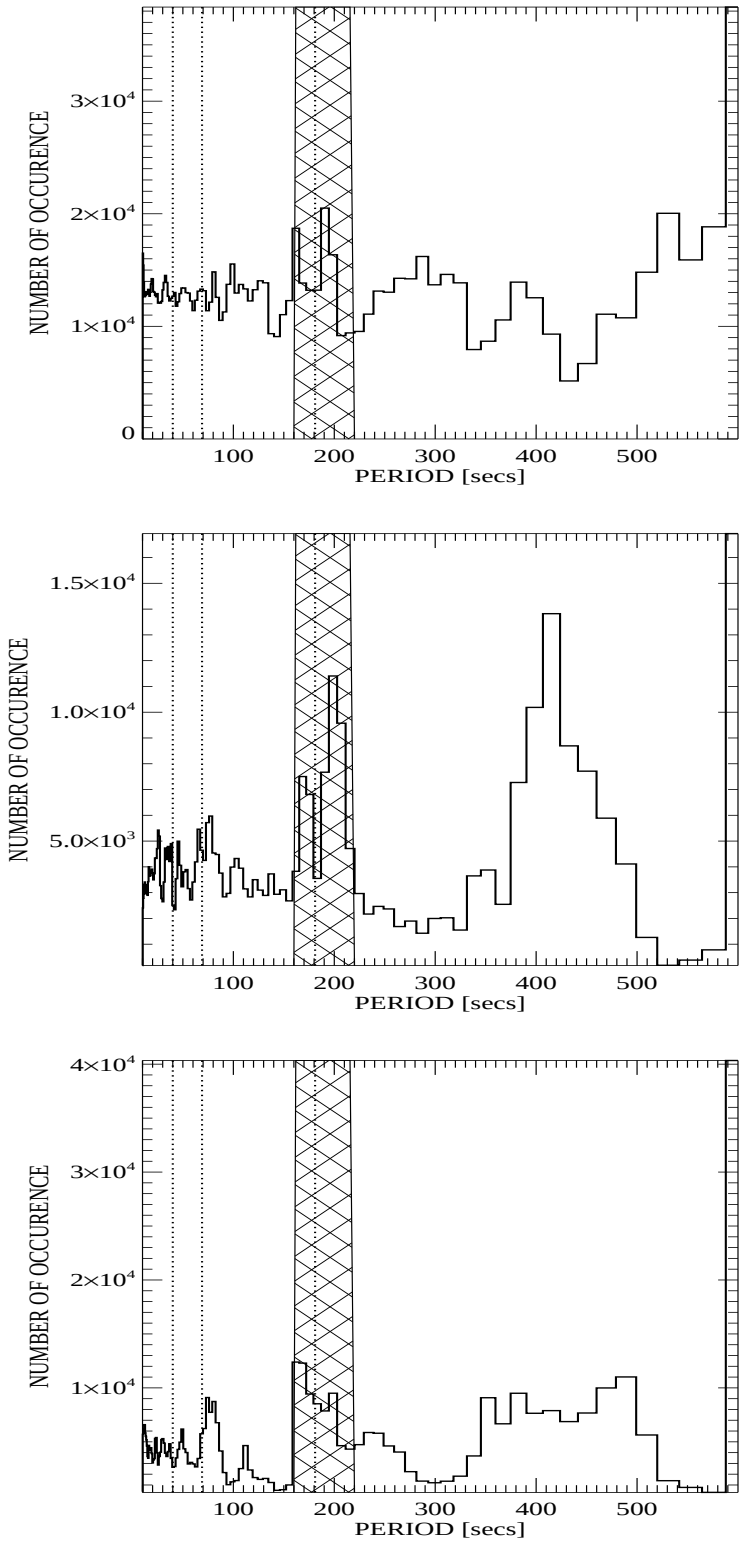

Figure 3. Histograms of the significant WT periods determined by the wavelet transformation of the radio-flux time series at all frequencies of the radio spectra (IZMIRAN (top), Phoenix-4 (middle), and Ondřejov (bottom)). The vertical-dotted lines show the periods found in UV observations (40, 69, and 181 seconds). A cross-hatched band marks the interval of periods around 181 seconds, considered for further detailed analysis (see Figures 4, 5, and 6).

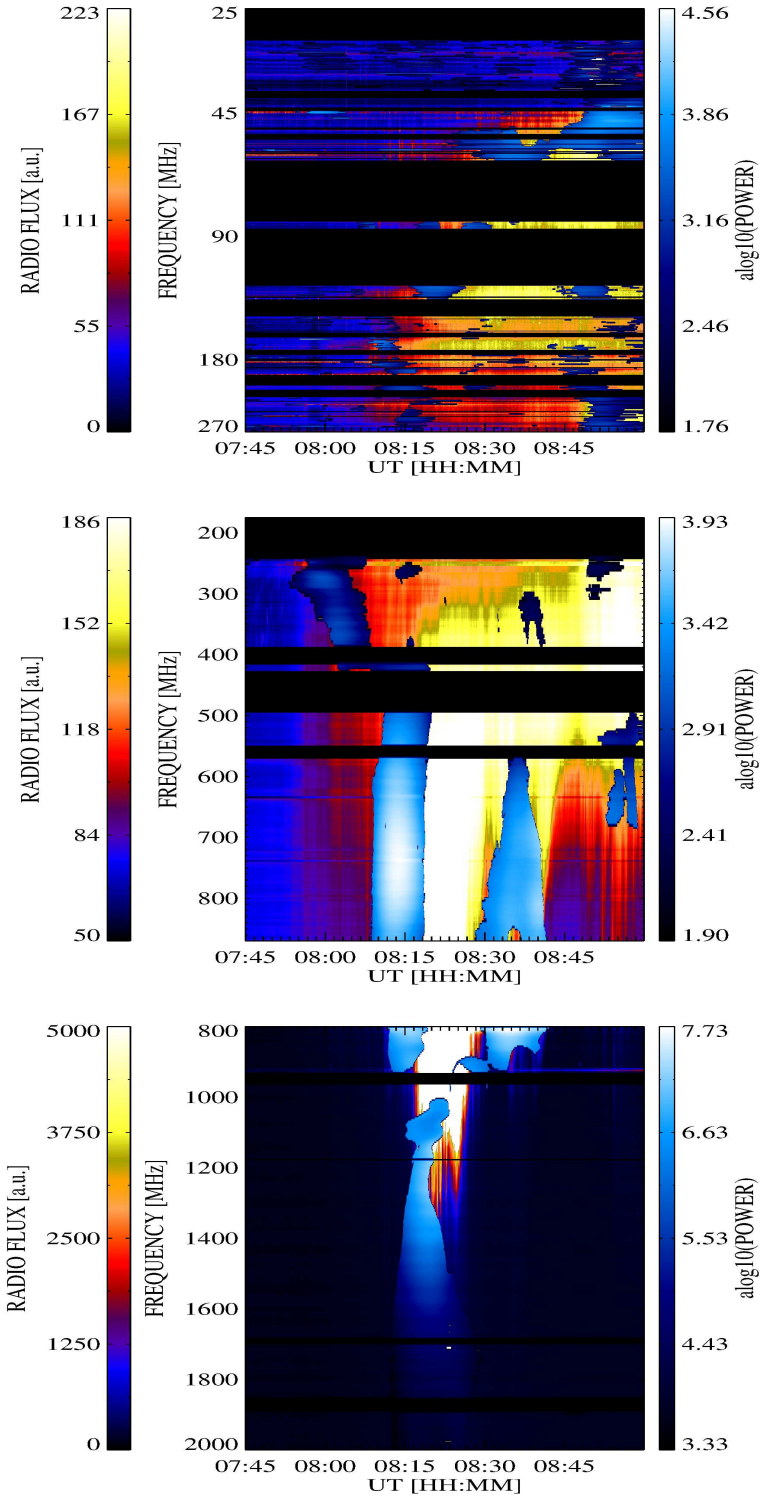

Figure 4. Radio spectra recorded by the IZMIRAN (*top*), Phoenix-4 (middle), and Ondřejov (bottom) radiospectrographs over-plotted by the light-blue areas, where the significant WT power for the period interval around 181 seconds (see the cross-hatched band in Figure 3) was found.

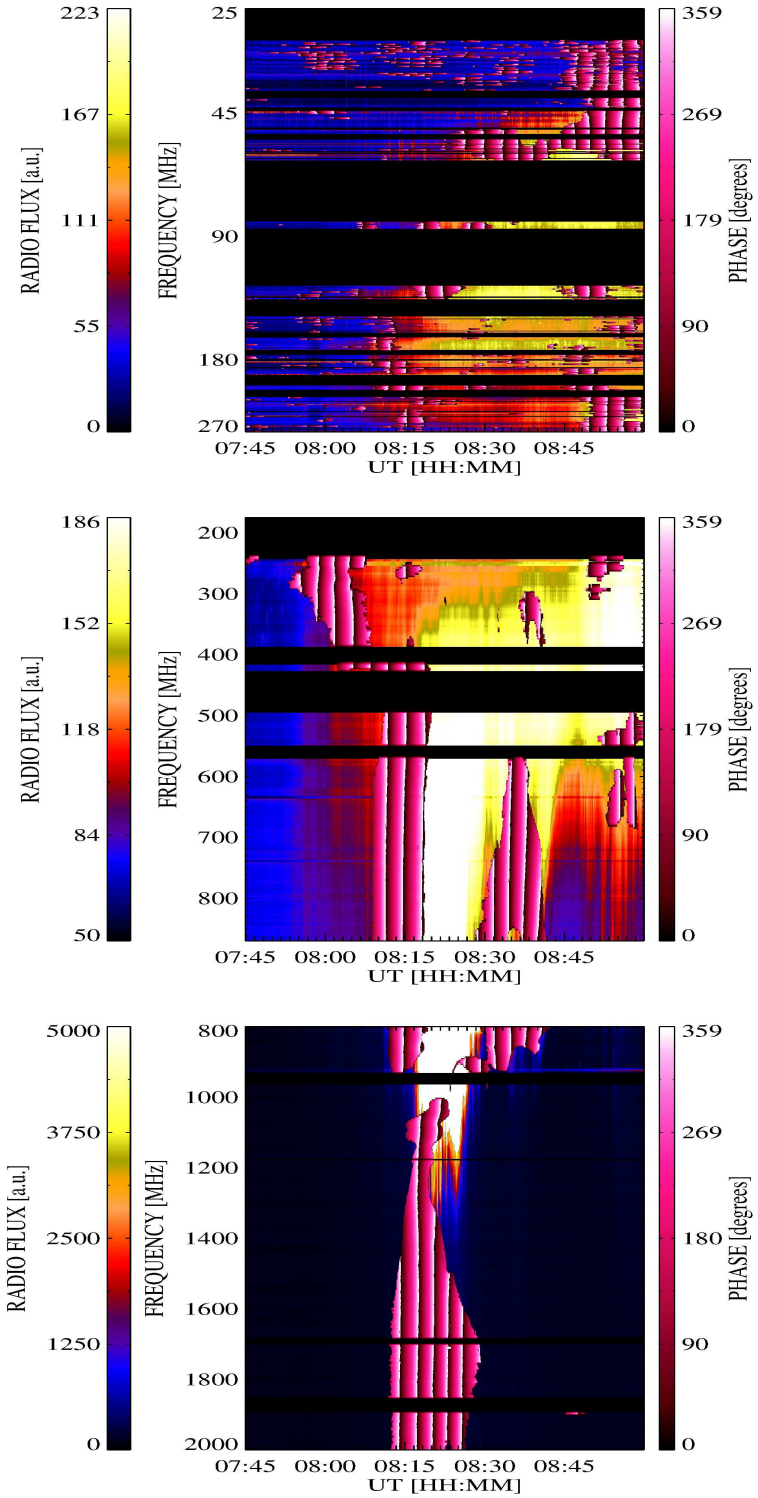

Figure 5. Radio spectra recorded by the IZMIRAN (top), Phoenix-4 (middle), and Ondřejov (bottom) radiospectrographs over-plotted by the areas as in Figure 4, but with the pink bands, showing the wave phase. The black borders of these bands indicate zero phase.

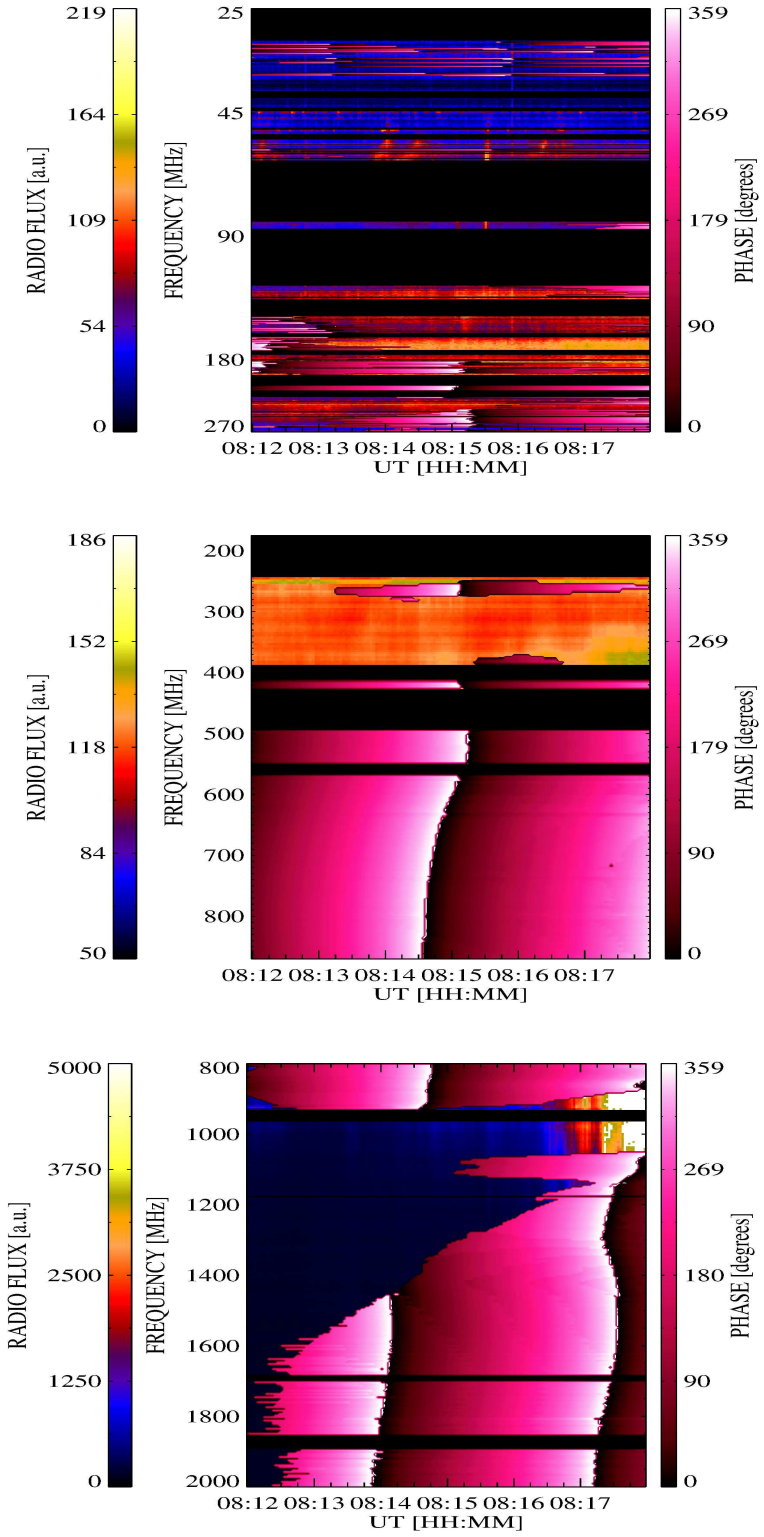

Figure 6. Radio spectra recorded by the IZMIRAN (top), Phoenix-4 (middle), and Ondřejov (bottom) radiospectrographs over-plotted by the areas of the WT phase (the pink bands) but just for the temporal interval 08:12 – 08:18 UT. The black borders of these bands indicate zero phase.

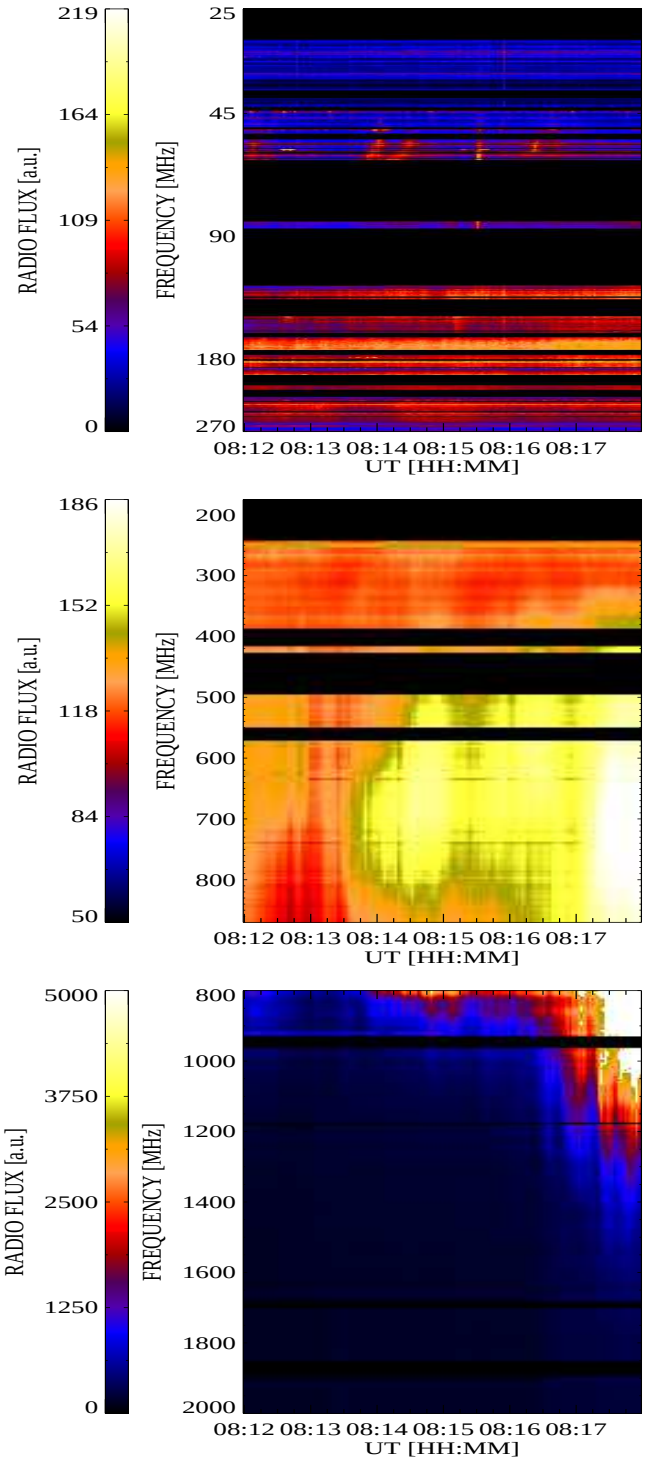

Figure 7. Original radio spectra recorded by the IZMIRAN (top), Phoenix-4 (middle), and Ondřejov (bottom) radiospectrographs without any overplot but just for the temporal interval 08:12 – 08:18 UT.